
Article:
Adamson, Hope, Simonov, Alexandr N, Kierzek, Michelina et al. (4 more authors) (2015) Electrochemical evidence that pyranopterin redox chemistry controls the catalysis of YedY, a mononuclear Mo enzyme. Proceedings of the National Academy of Sciences of the United States of America. pp. 14506-14511. ISSN: 1091-6490

https://doi.org/10.1073/pnas.1516869112

Electrochemical Evidence that Pyranopterin Redox Chemistry Controls the Catalysis of YedY, a Mononuclear Mo Enzyme

Hope Adamson[a], Alexandr N. Simonov[b], Michelina Kierzek[c], Richard Rothery[c], Joel H. Weiner[c], Alan M. Bond[b], Alison Parkin[a,1]

[a]Department of Chemistry, University of York, Heslington, York YO10 5DD, United Kingdom; [b]School of Chemistry, Monash University, Clayton, Victoria 3800, Australia; and [c]Department of Biochemistry, 474 Medical Science Building, University of Alberta, Edmonton, Alberta T6G 2H7, Canada

Submitted to Proceedings of the National Academy of Sciences of the United States of America

A longstanding contradiction in the field of mononuclear Mo enzyme research is that small-molecule chemistry on active site mimic compounds predicts ligand participation in the electron-transfer reactions, but biochemical measurements only suggest metal-centred catalytic electron transfer. With the simultaneous measurement of substrate turnover and reversible electron-transfer which is provided by Fourier transformed alternating current voltammetry we show that *Escherichia coli* YedY is a mononuclear Mo enzyme which reconciles this conflict. In YedY, addition of three-protons and three-electrons to the well-characterised "as-isolated" Mo(V) oxidation state is needed to initiate the catalytic reduction of either dimethyl sulfoxide or trimethylamine N-oxide. Based on comparison with earlier studies and our UV-vis redox titration data, we assign the reversible one-proton and one-electron reduction process centred around +174 mV *vs* SHE at pH 7 to a Mo(V) to Mo(IV) conversion but ascribe the two-proton and two-electron transition occurring at negative potential to the organic pyranopterin ligand system. We predict that a dihydro to tetrahydro transition is needed to generate the catalytically active state of the enzyme. This is a novel mechanism, suggested by the structural simplicity of YedY, a protein in which Mo is the only metal site.

Fourier transformed alternating current voltammetry | mononuclear molybdenum enzyme | protein film electrochemistry | pyranopterin | YedY

Introduction

Most living species require a Mo enzyme (1) and apart from nitrogenase all of these Mo-containing proteins are part of the large family of "mononuclear Mo" enzymes. The general ability of mononuclear Mo enzymes to catalyse two-electron oxygen atom transfer reactions has been attributed to the Mo(IV)/Mo(V)/Mo(VI) oxidation-state cycling of the active site, and this mechanism is a common part of Undergraduate syllabuses (1, 2). *Escherichia coli* YedY is a mononuclear Mo enzyme (3) and, based on sequence homology, the majority of sequenced Gram-negative bacterial genomes encode a YedY-like protein (3-5). Uniquely for a mononuclear Mo enzyme, it has not been possible to form the YedY Mo(VI) state in experiments using ferricyanide as an oxidising agent, and an unusually positive reduction potential for the Mo(V/IV) transition (+132 mV *vs.* SHE at pH 7) was determined from EPR experiments (6). Although the physiological substrate of YedY is unknown, a possible role in the reduction of reactive nitrogen species is suggested by experiments on the pathogen *Campylobacter jejuni*, where deletion of the Cj0379 YedY-homologue generated a mutant which is deficient in chicken colonization and has a nitrosative stress phenotype (4). YedY catalysis can be assayed by measuring the two-electron reduction of either dimethyl sulfoxide (DMSO) or trimethylamine N-oxide (TMAO) (3) but the inaccessibility of the YedY Mo(VI) means the enzyme mechanism does not proceed via the common two-electron Mo-redox cycle. In small molecule analogues of mononuclear Mo enzymes the pterin ligands are described as "non-innocent" meaning that the redox processes could be ligand or metal based (7). This study explores the possibility that ligand-based redox chemistry plays a role in YedY catalysis.

YedY has been structurally characterised via both X-ray crystallography and X-ray absorption spectroscopy (XAS) (3, 8, 9). In most mononuclear Mo enzymes, heme groups and iron sulphur clusters are found within the same protein as the Mo centre, but the only metal site in YedY is Mo, making this enzyme a helpfully simple system for studying redox chemistry (Fig. 1) (1, 3). Within the active site the X-ray structure was interpreted to show Mo(V) in a square pyramidal environment (3), identical to other members of the "sulfite oxidase" family of mononuclear Mo enzymes. In contrast, XAS has suggested a pseudooctahedral Mo center (8, 9) with an additional O (from Glu104) or N (from Asn45) axial ligand coordinating *trans* to the apical oxo group (Fig. 1) (8). The equatorial ligation is provided by one oxygen-containing ligand and three sulphur donor atoms, one provided by cysteine (Cys102) and two from the pyranopterin cofactor which binds to the Mo in a bidentate fashion via the enedithiolate side chain (3).

A 2012 computational study provided evidence that two different oxidation states can be accessed by protein-bound pyranopterin ligands (10). Conformational analysis and electronic

Significance

The mononuclear Mo enzymes are ubiquitous throughout life and the notion that their activity arises from Mo(VI/V/IV) redox cycling is a central dogma of bioinorganic chemistry. We prove that YedY, a structurally simple mononuclear Mo enzyme, operates via a strikingly different mechanism: the catalytically active state is generated from addition of three-electrons and three-protons to the Mo(V) form of the enzyme, suggesting for the first time that organic-ligand based electron-transfer reactions at the pyranopterin play a role in catalysis. We showcase Fourier transformed alternating current voltammetry as a technique with powerful utility in metalloenzyme studies, allowing the simultaneous measurement of redox catalysis *and* the underlying electron-transfer reactions.

Reserved for Publication Footnotes

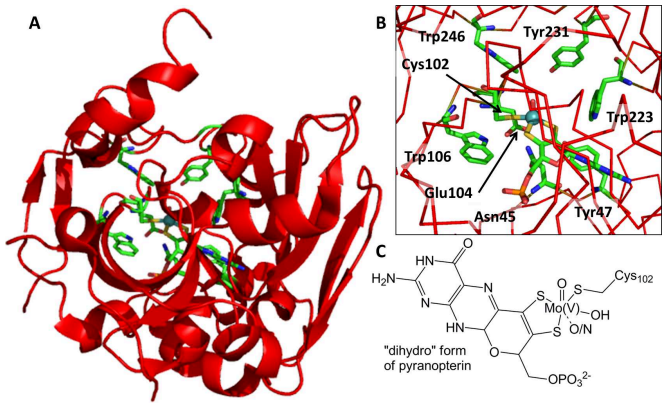

Fig. 1. Structure of *Escherichia coli* YedY. (A & B) The protein structure, PDB 1XDQ (3). **(C)** The active site in the as-isolated Mo(V) state containing the "dihydro" form of pyranopterin.

structure calculations were used to assign redox states to the pyranopterin ligands in all known mononuclear Mo enzyme structures (10). It was concluded that while enzymes from the sulfite oxidase family (such as YedY) contain pyranopterin ligands in the "dihydro" form, the xanthine dehydrogenase family of enzymes contain the two proton, two electron more reduced "tetrahydro" form of the pyranopterin (10).

Traditionally, redox-potential measurements of enzymes have required substrate-free conditions to either permit a solution equilibrium to be established (spectroscopic redox titrations) or to prevent catalytic signals from masking the non-catalytic response (film electrochemistry). Fourier transformed alternating current voltammetry (FTacV) is a technique which offers the ability to measure catalytic chemical redox reactions and reversible electron transfer processes in a single experiment (11, 12). In the FTacV measurement, a large amplitude sine wave of frequency f is superimposed on a linear voltage-time sweep (11, 13-15) and the resulting current-time response is measured and then Fourier transformed (FT) into the frequency domain to give a power spectrum of harmonic contributions at frequencies f, $2f$, $3f$ etc. Band selection of the individual harmonics followed by inverse FT resolves the data back into the time domain. The higher harmonic components only arise from fast, reversible redox reactions, devoid of catalysis and baseline contributions, but the aperiodic (dc) component ($f = 0$) gives the same catalytic information as a traditional direct current cyclic voltammetry (dcV) experiment, and can therefore show catalytic turnover (13, 14, 16).

In this study we both discover novel mononuclear Mo enzyme redox chemistry as well as demonstrate the significant advantages of using FTacV to probe the mechanism of a redox active enzyme.

Results

Electrochemical Observation of Two Redox Transitions by YedY. We prove that YedY can reversibly form three different oxidation states, i.e. the enzyme can undergo two different redox transitions. This is shown in Fig. 2A which contains dcV YedY electrochemistry data measured under conditions of pH 7, 25°C. The enzyme has been adsorbed onto the surface of the electrode and the signals which are observed are typical for non-catalytic redox-enzyme "film" electrochemistry (SI Appendix (Fig. S1)) (17). In Fig. 2A, both enzyme-redox transitions are visible as "peak" Faradaic signals at around +170 mV and -250 mV (control experiments confirm that these signals are not present with a YedY-free electrode). The YedY signals were stable over at least 20 continuous 100 mVs^{-1} cyclic voltammograms but only one scan is shown for clarity.

A significant limitation of the protein film dcV technique is that the Faradaic non-catalytic enzyme signals are very small in

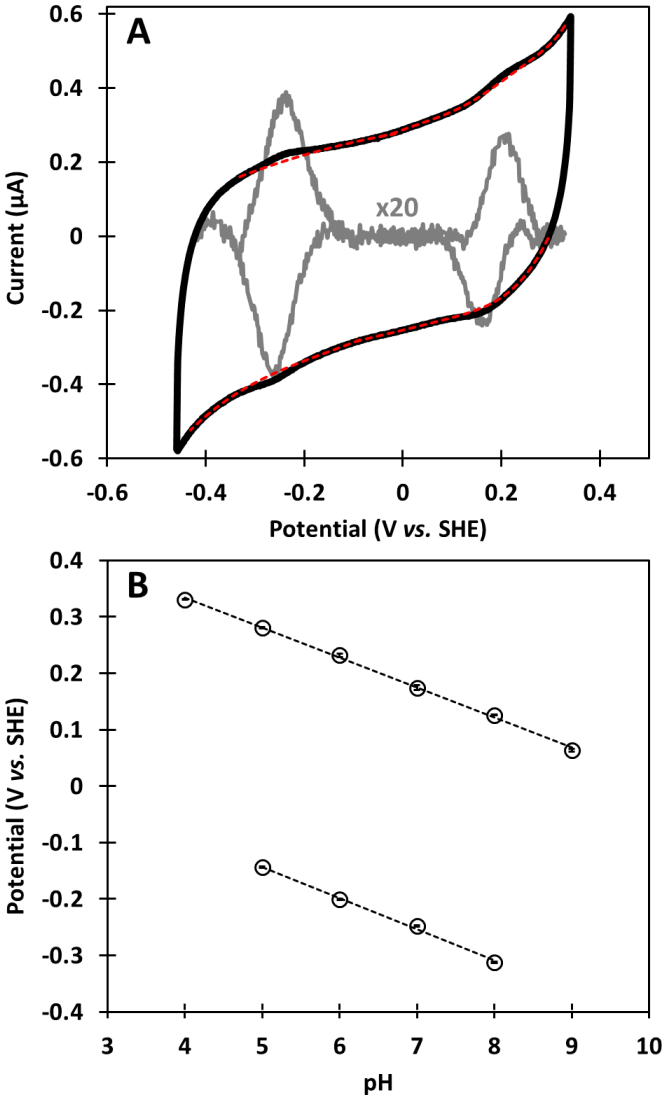

Fig. 2. Redox transitions of YedY measured by dcV at a scan rate of 100 mV s^{-1}. (A) A cyclic voltammetry measurement of YedY in 50 mM MES buffer, pH 7 is shown by the black solid line. The baseline is shown by the red dashed line, the baseline subtracted signal (scaled by a multiplication factor of 20) is depicted by the gray solid lines. **(B)** pH dependence of peak midpoint potentials derived from voltammetry experiments conducted in 50 mM buffer solution of either acetate (pH 4 and 5), MES (pH 6 and 7) or Tris (pH 8 and 9). Error bars shown within data point circles reflect the standard error calculated from at least 3 repeat experiments. Other conditions: stationary electrode, and temperature 25°C.

relation to the "background" signal from the non-Faradaic (double layer charging) electrode process. To permit analysis of the YedY-only redox chemistry we have computed the non-Faradaic response using a polynomial function and then subtracted this from the experimental data to give pure Faradaic data. The baseline-subtracted signals thus obtained are scaled by a 20-fold multiplication factor in Fig. 2A. From Fig. 2A the integrated area of the baseline subtracted negative potential process, centred around -250 mV, is approximately 1.8 times larger than the integrated area of the baseline subtracted positive potential process centred around +170 mV. We therefore conclude that almost twice as many electrons are passed in the negative potential redox transition relative to the positive potential redox transition.

As shown in the SI Appendix (Fig. S2B), the redox transition measured for YedY at positive potential is well modelled by a

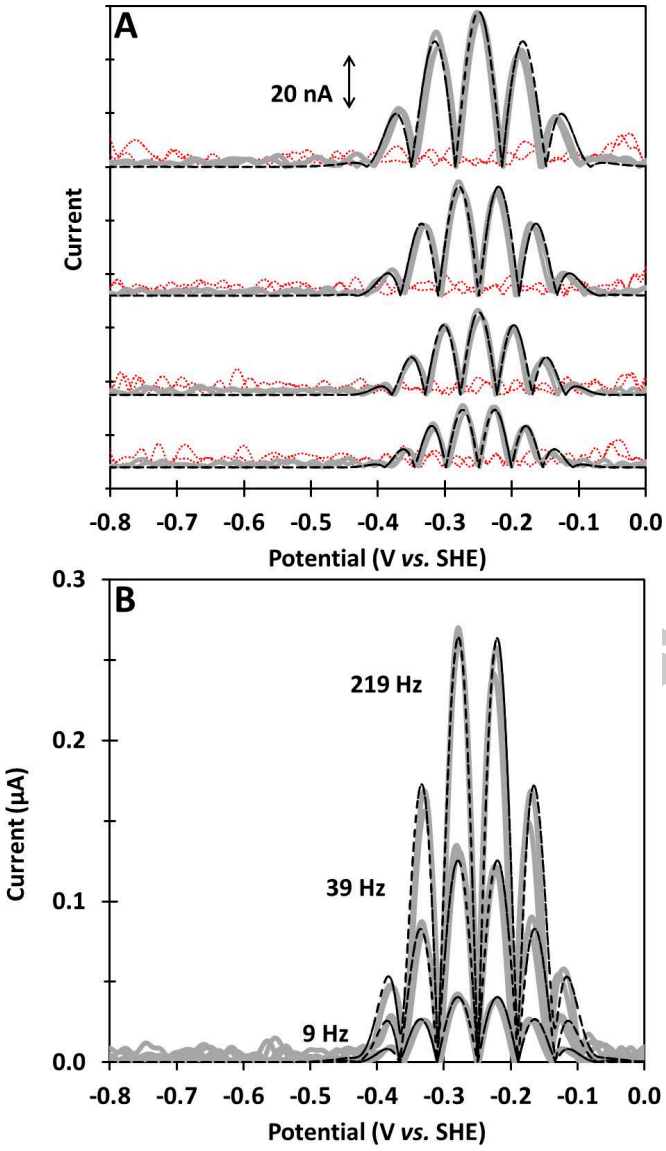

Fig. 3. FTacV measurements of the YedY two-electron redox transition. (A) Gray solid lines show, in descending order, the 7th, 8th, 9th and 10th ac harmonic signals measured for YedY using FTacV with a frequency of 9 Hz. The response from a bare (YedY-free) graphite electrode under the same conditions is shown by light red dotted line. **(B)** Gray solid lines compare the 8th ac harmonic from YedY FTacV experiments at different frequencies, as denoted in the graph. **(A & B)** Black dashed lines depict simulated data for a $1e^-$ + $1e^-$ mechanism with parameters $E^0_{app(1)}$ = −239 mV $E^0_{app(2)}$ = −261 mV, $(k^0_1)_{app}$ = $(k^0_2)_{app}$ = $2{\cdot}10^4$ s^{-1}, R_u = 50 Ω, polynomial capacitance, Γ = 1.15 pmol cm^{-2} (9 Hz), Γ_{app} = 0.86 pmol cm^{-2} (39 Hz), Γ_{app} = 0.66 pmol cm^{-2} (219 Hz). Other experimental conditions: scan rate 15.83 mVs^{-1}, amplitude 150 mV, buffer solution of 50 mM MES and 2 M NaCl, pH 7, 25°C.

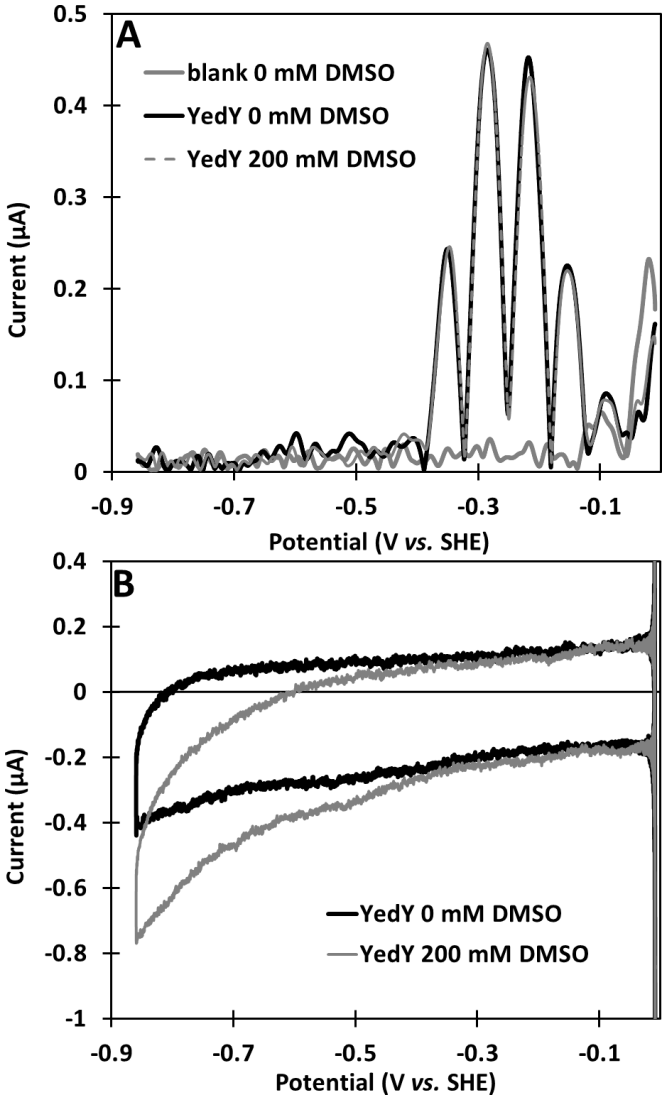

Fig. 4. FTacV of YedY in the presence and absence of DMSO substrate. (A) 6th harmonic component of a 219 Hz FTacV experiment on YedY in the absence (black solid line) and presence (gray dashed line) of 200 mM DMSO. The response of a blank or bare (YedY-free) graphite electrode in the absence of DMSO, measured using the same FTacV parameters, is shown by the gray solid line. **(B)** The aperiodic dc component of the same FTacV experiment on YedY in the absence (black solid line) and presence (gray solid line) of DMSO. Other conditions: scan rate 15.83 mVs^{-1}, amplitude 150 mV, buffer solution of 50 mM MES and 2 M NaCl, pH 7, 25°C and stationary electrode.

Nernstian one-electron process (equivalent to a peak width at half height, δ, of 90 mV) with a pH 7 mid-point potential $E_{m,7}$ = +174 ± 4 mV. We attribute this process to the Mo(V/IV) redox transition. Our assignment of the positive potential redox process as a metal-based transition is supported by UV-vis solution spectroelectrochemistry measurements made from 750 to 320 nm under an atmosphere of Ar and shown in the SI Appendix (Fig. S3). As-purified YedY, known to be in the Mo(V) state, exhibits two peaks in the optical spectrum (6, 18): a broad absorbance centred at 503 nm and another at approximately 360 nm. Upon lowering the solution potential from +0.21 V to −0.09 V, i.e. passing through the positive potential redox transition, both spectral signals are bleached, indicating a metal-based reduction. These spectral changes can be reversed by raising the potential back to +0.21 V. No spectral changes accompany the negative potential redox reaction, i.e. no UV-vis changes are measured when the solution potential is stepped between -0.44 and -0.09 V.

Using film electrochemistry, there is no evidence of any further redox transitions at more positive potentials, even when the potential range is extended to the solvent/electrode limit (SI Appendix (Fig. S4)), so in agreement with other techniques, we also cannot observe a Mo(VI/V) redox transition.

Analysis of the negative potential baseline-subtracted dcV waveshape shown in the SI Appendix (Fig. S2C) suggests a cooperative, non-simultaneous two electron charge transfer process, i.e. one electron is transferred and then a second electron follows onto the same centre (19-22). We measure $E_{m,7}$ = -248 ± 1 mV but using dcV it is very difficult to derive more precise mechanistic

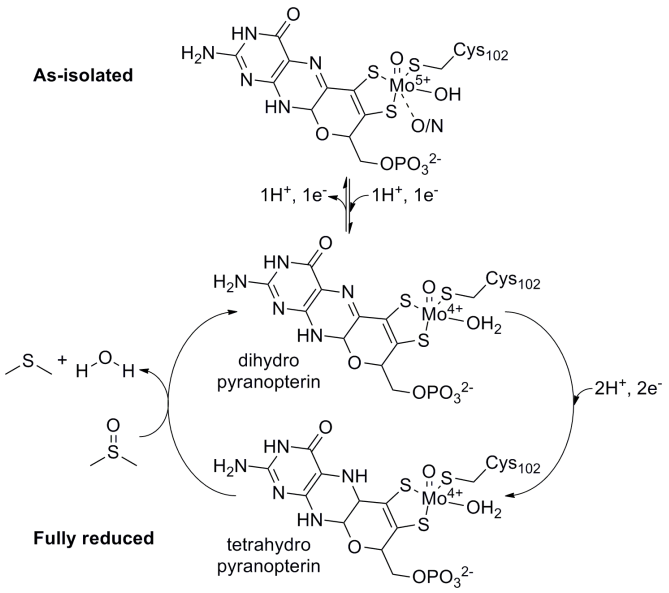

Fig. 5. Proposed redox state cycling of YedY.

information regarding the separate one-electron processes which combine to give the "envelope" signal.

Experiments at different pH reveal that the E_m values for the Mo(V/IV)-assigned reaction and the negative potential redox processes change by −53 and −55 mV per pH unit, respectively (Fig. 2B), close to the −59 mV per pH unit expected for a one-proton per electron process at 25°C (23). "Trumpet plots" of the reductive and oxidative peak potentials *vs.* scan rate show greater peak separation at lower scan rates for the Mo(V/IV) signals compared to the negative potential transition, suggesting that the Mo-based redox process has a slower electron transfer rate (SI Appendix (Fig. S5)) (24). Combining all the dcV information, we suggest a $1H^+ + 1e^-$ process for the Mo(V/IV) transition and a faster $2H^+ + 2e^-$ process for the negative potential transition, over the pH range measured.

Fourier Transformed ac Voltammetry (FTacV) of YedY. Analogous to the dcV experiment shown in Fig. 2, FTacV was used to interrogate YedY redox chemistry over a wide potential range and this is shown in the SI Appendix (Fig. S6). There are two significant differences between the two results; firstly, relative to dcV, the signal-to-background response of YedY at around -250 mV is much larger in the higher harmonic components of the FTacV measurements; secondly, whereas in dcV the peak area for the negative potential YedY signal is approximately double the peak area of the Mo(V/IV) signal, in FTacV the Mo(V/IV)-assigned signal is not visible above the noise. The fact that very little Mo(V/IV) signal is observed means that the 9 Hz frequency applied in the FTacV outpaces Mo-based electron transfer processes and we can therefore state that YedY's negative potential electron transfer processes is much faster than the Mo(V/IV) redox transition. Based on analysis of the FTacV signals we define the Mo(V/IV) process as a quasi-reversible electron transfer reaction with an apparent heterogeneous charge transfer rate k^0_{app} of less than 10 s^{-1}, consistent with analysis of dcV trumpet plot data which suggests $k^0_{app} = 3 - 6\ s^{-1}$.

In order to learn more about the negative potential process, Fig. 3A shows 9 Hz FTacV measurements focussed on the YedY reversible redox transition centred at around -250 mV. At least 12 harmonic components are detected and, in stark contrast to dcV, no baseline subtraction is required prior to analysis of the higher harmonic signals because YedY-free controls confirm there is negligible baseline contribution from a bare electrode. The potentials of the central maxima of the odd harmonics and the central minima of the even harmonics provide a direct measure of the midpoint potential and these values agree with the baseline subtracted dcV E_m data. Similar to changing the scan rate in dcV, changing the frequency in FTacV provides a qualitative means of assessing the electron transfer rate. As shown in Fig. 3B, when the same negative potential range is interrogated using a range of frequencies, well defined ac harmonics are observed up to 219 Hz, indicating that the low potential YedY redox reaction involves extremely fast electron transfer.

Electrocatalytic Activity of YedY. The ability of FTacV to separately resolve catalytic and electron transfer steps in a single experiment is shown in Fig. 4. Solution assays have shown that YedY catalyses the reduction of N- or S-oxides with concomitant oxidation of reduced benzyl viologen (3). The enzyme has the largest specificity constant, k_{cat}/K_M, for the substrates DMSO and TMAO, where k_{cat} refers to the catalytic turnover rate and K_M denotes the Michaelis constant (3). When YedY is adsorbed onto a graphite electrode and then placed in a solution of DMSO, the negative catalytic reduction current, revealed by the dc component of the data (Fig. 4B), steadily increases as the electrode potential is lowered below approximately −0.3 V at pH 7 ("control" enzyme-free electrode experiments in the presence of DMSO show no reductive current, see SI Appendix). In contrast, the aperiodic component resembles a "blank" electrode in the presence of YedY but absence of substrate (Fig. 4B). The reduction potential for DMSO is +160 mV at pH 7 and work by Heffron et al. shows that the enzyme *E. coli* DMSO reductase is capable of reducing DMSO at more positive voltages than YedY (25). In Fig. 4B the "onset potential", i.e. the electrochemical voltage required to initiate YedY-catalysed DMSO reduction, is therefore an enzyme-specific property and not a substrate related behaviour.

The 6th harmonic signal for YedY, shown in Fig. 4A, is unchanged in the presence or absence of 200 mM DMSO, showing that substrate has not affected the electron transfer properties of the negative potential redox process: it remains very clearly distinguishable, revealing the redox potential without any need for background subtraction. Comparison between the high harmonic data in the presence and absence of substrate therefore suggests that the negative potential two-electron, two-proton reduction process generates the catalytically active state of YedY, since catalysis does not commence until the potential is sufficiently negative for this reaction to have occurred. Experiments at different pH further support the hypothesis that the most reduced state of the enzyme reacts with substrate because the onset potential of YedY-catalysed DMSO-reduction changes between pH 5 and 8 in exactly the same way as the potential of the two-electron non-catalytic redox signal (SI Appendix (Fig. S7)). Data extracted from experiments at pH 7 and different DMSO concentrations also corroborate published solution assay measurements with K_M = 35 ± 5 mM at pH 7, 25 °C and k_{cat} = 4.2 ± 0.9 s^{-1} at −359 mV, pH 7, 25 °C (SI Appendix (Fig. S8)) (3, 8, 26). Electrocatalytic experiments have also been conducted using TMAO as a substrate; these are shown in the SI Appendix (Fig. S9). With TMAO as a substrate we again observe that the onset potential of YedY catalysis is approximately -0.3 V at pH 7, far more negative than the equilibrium redox potential for the substrate (TMAO has reduction potential +130 mV at pH 7 (27)).

Simulation of the FTacV data. Simulation of the FTacV data makes it possible to harness the technique's ability to provide a quantitative measure of electron transfer rates and deconvolution of separate redox potentials in a single experiment, insight that we cannot access with dcV (22). Fig. 3A shows simulations of the FTacV data using the $1e^- + 1e^-$ mechanism described in the SI Appendix. The same parameters were used to simulate all the harmonic signals. To minimise the parameter space used

in simulations the value for uncompensated resistance, R_u, was derived from a separate impedance spectroscopy measurement and Γ_{app}, the apparent coverage of enzyme on the electrode, was estimated from dcV measurements. Both electron transfer steps exhibit fast kinetics as reflected by $(k_1^0)_{app}$, $(k_2^0)_{app}$= $2.0 \cdot 10^4$ s^{-1} used in simulations. To achieve a close agreement to experimental data the apparent reversible potentials of the two sequential one-electron transfers must be similar and $(E_1^0)_{app}$= −239 mV and $(E_2^0)_{app}$ = −261 mV are used to produce data in Fig. 3. The charge transfer coefficient α was always assumed to be 0.5 and its exact value could not be determined as the simulations are insensitive to α at these very high electron transfer rates. As expected, simulations using Marcus theory rather than Butler Volmer theory made no difference under these reversible conditions. As shown in the SI Appendix we confirmed that different redox reaction models will not simulate the data, confirming that the low potential YedY redox reaction is neither a $1e^-$ reaction (Fig. S10) or a simultaneous $2e^-$ transfer mechanism (as opposed to a stepwise $1e^-$ + $1e^-$ reaction, Fig. S11).

When simulating the FTacV data obtained from experiments at different frequency (Fig. 3B), all the same parameters were used except for the enzyme-electrode coverage value, Γ_{app}, which was lowered with increasing frequency from 1.15 pmol cm^{-2} in the first 9 Hz measurement, to 0.615 pmol cm^{-2} for 519 Hz (Fig. 3B and SI Appendix (Fig. S12)). This trend did not reflect true enzyme desorption because a final measurement at 9 Hz yielded data that was best simulated using Γ_{app} of 0.9 pmol cm^{-2}. As described in a recent theoretical study (28), kinetic dispersion, meaning that different enzyme orientations on the electrode surface have different electron transfer rates (k^0_{app}), is believed to be the major reason that Γ_{app} decreases as the frequency increases. Dispersion is a common observation in protein film electrochemistry measurements (29).

Discussion

We present dcV and FTacV data that prove that *E. coli* YedY forms three stable oxidation states. Relative to the well-characterised Mo(V) form of the enzyme, formation of the catalytically active state requires addition of three electrons and three protons and we summarise our proposed mechanism in Fig. 5. We assign the YedY redox transition which has $E_{m,7}$ = +174 ± 4 mV to the Mo(V/IV) process and ascribe the redox transition with $(E_1^0)_{app}$= −239 mV and $(E_2^0)_{app}$ = −261 mV to a pyranopterin dihydro-tetrahydro interconversion.

Using spectroelectrochemistry it has been demonstrated that application of -0.09 V is sufficient to bleach the absorbance peaks observed in UV-vis spectra of the as-isolated, Mo(V), enzyme. The disappearance of the absorbance centred at 503 nm is consistent with our assignment of the positive potential redox process being Mo-based; dithiolene-S ligand to metal charge transfer processes give rise to this spectral feature so it should be a reporter signal for changes to the metal redox state (18). Both dcV trumpet plot data and low intensity FTacV harmonic currents indicate that the Mo(V/IV) redox reaction has a slow electron transfer rate, from 3 – 6 s^{-1}, which suggests structural reorganisation. This correlates with the XAS mechanism that six coordinate Mo(V) is reduced to a five coordinate Mo(IV) species (9).

Varying the pH from 4 to 9 causes the electrochemically-determined E_m(Mo(V/IV)) value to decrease by 53 mV per pH unit which indicates a one-electron, one-proton transition in agreement with the proposed XAS mechanism: Mo(V)−OH + $1H^+$ + $1e^-$ → Mo(IV)−OH_2 (9). There is a discrepancy between the midpoint potentials we measure using electrochemistry and those reported from an EPR redox titration, with respective $E_{m,7}$ values of +174 mV and +132 mV (6). The EPR data is also pH-independent over a range of pH 6-8 (6). Whereas the dcV electrochemical data could be accurately simulated as a one-electron Nernstian process, the EPR Nernst plots were fit as physically impossible 1.3 and 1.63 electron processes for the oxidative and reductive titrations, respectively. As noted in the EPR study (6), the complex spectroscopic data is difficult to interpret and we suggest that the disparity in midpoint potential values may reflect this challenge. We also note that the electrochemical and EPR redox potential measurements are made on very different timescales as protein film electrochemistry affords the advantage of "wiring" the enzyme to the electrode, permitting rapid potential control, whereas achieving solution redox potential equilibration for EPR requires many minutes.

Our experiments at highly oxidising potentials confirm the unusual stability of the YedY Mo(V) state with respect to oxidation, setting a limiting value of $E_{m,7}$(Mo(IV/V)) > +600 mV. The Mo(VI) oxidation state is therefore defined as physiologically irrelevant and thus plays no direct role in a catalytic reaction mechanism.

FTacV permitted simultaneous measurement of the putative pyranopterin redox transition *and* catalysis. The onset potential for enzymatic reduction of either DMSO or TMAO is more negative than the redox potential of either substrate (27) and instead correlates with the pyranopterin-assigned two-electron, two-proton reversible redox transition across the pH range 5 to 8. We assign this process to the pyranopterin cofactor because the structural simplicity of YedY is such that there are no other putative redox active centres apart from the Mo (3). In sulfite oxidase fold enzymes such as YedY, which is crystallised in the Mo(V) oxidation state, the geometry of the pyranopterin is consistent with a 10,10a-dihydro form (10); in Fig. 5 we show the three-electron, three-proton reduced catalytically active Mo(IV) form of the enzyme with a tetrahydro pyranopterin ligand. We have chosen to display the two-electron reduced pyranopterin ligand in a ring-closed tetrahydro state because this is consistent with the structure found most frequently at the active site of Mo-containing enzymes (10). However it should be noted that an alternative, ring-opened confirmation exists at the same oxidation state level (7). For simple pterins, reversible two-electron and two-proton transitions between tetrahydro and dihydro forms are well known, as is further oxidation of the dihydro state, so pyranopterin redox reactions would be expected on the basis of chemical analogues (7, 30). It has been proposed that a nitrate reductase undergoes reversible enzymatic inactivation under oxidising conditions because the pyranopterin converts from the tetrahydro to the dihydro state, however all the substrate reactions were still thought to be solely metal based (31). Our experiments therefore provide the first evidence of catalytically relevant pyranopterin redox chemistry (Fig. 5).

It is not possible to conclude if the two electrons for substrate reduction are supplied directly by the pyranopterin or if reduction of the pyranopterin ligand activates the Mo in such a way as to promote changes to the metal redox state catalysis. In the reduced tetrahydro state, the dithiolene chelate of a pyranopterin has increased electron donating ability to Mo, which will decrease the Mo reduction potentials, because relative to the oxidised dihydro form π-delocalisation is lost between the dithiolene chelate and the pterin ring (10). This could make the Mo(VI) state indirectly accessible. There is no conclusive structural information about how the substrate coordinates to YedY, XAS experiments on the Mo(V) state at pH 8 showed a possible long-range coordination of TMAO to Mo, but DMSO coordination was undetectable (8). To probe substrate binding, future experiments would need to be conducted under reducing conditions.

Comparison of Fig. 2 and Fig. 3 demonstrates how the complete absence of background current in the higher harmonic FTacV YedY signals results in much better defined non-catalytic

redox peaks, overcoming the need for the significant baseline subtraction which is required in analysis of dcV data. Simulation of the higher harmonic YedY FTacV responses has also provided detailed information on the thermodynamics (apparent E^0), kinetics (apparent k^0 at E^0_{app}) and mechanism of the pyranopterin-assigned electron transfer. Simulation of the FTacV data suggests that the pyranopterin redox reaction proceeds via a sequential $1e^- + 1e^-$ process and is extremely fast ($(k^0_1)_{app}$, $(k^0_2)_{app} \geq 2.0\ 10^4\ s^{-1}$). Previous measurements of biological electron transfer rates using FTacV have been predominantly on metal centres and much slower electron transfer rates have been calculated (13, 16, 22, 32-34), supporting our conclusion that the delocalised organic ligand is the site for oxidation state changes.

Materials and Methods

Samples and Solutions. *Escherichia coli* YedY was prepared as described previously (3, 6) and stored in a buffer solution of 20mM 3-(N-morpholino)propanesulfonic acid (MOPS), pH 7 which was also used for the UV-vis spectroelectrochemical experiments. For film-electrochemistry experiments, a protein concentration of approximately 10 mg mL^{-1} was used, for spectroelectrochemistry the protein concentration was 5.3 mg mL^{-1}.

All film electrochemistry experiment solutions were prepared using deionised water from a Pur1te Select water purification system (7.4 MΩ cm). The buffer salts were either: pH 4 to 5, 50 mM acetate; pH 6 to 7, 50 mM 2-(N-morpholino)ethanesulfonic acid (MES); pH 8 to 9, 50 mM tris(hydroxymethyl)aminomethane (Tris). The pH was adjusted by addition of NaOH or HCl for MES and Tris buffers and acetic acid for acetate buffer. Additional supporting electrolyte of NaCl was used where stated. Dimethyl sulfoxide (DMSO, Fisher) or trimethylamine N-oxide (TMAO, Sigma) were used as enzyme substrates. All solids were of at least 99% purity.

Protein Film Electrochemistry Apparatus and Methods. Direct current voltammograms were measured with an Ivium CompactStat potentiostat and FTacV measurements were performed using custom made instrumentation described elsewhere (11, 14). All electrochemical experiments were performed under a N_2 atmosphere in a glove box (manufactured by University of York Chemistry Mechanical and Electronic Workshops). A conventional three-electrode setup was used with the pyrolytic graphite edge working electrode (0.03 cm^2 geometric area, made in-house), Pt wire counter electrode (Advent research materials) and saturated calomel reference electrode (Scientific laboratory supplies) all located in an all-glass, water-jacketed electrochemical cell (manufactured by University of York Chemistry Glassblower). The connection to the working electrode was made via an OrigaTrod electrode rotator and the electrode was rotated during dcV catalysis experiments to ensure that substrate and product mass transport did not limit the enzyme activity. The electrode was not rotated for FTacV catalysis experiments. All experiments were performed at 25 °C and all potentials have been converted to the standard hydrogen electrode (SHE) scale using the correction +241 mV at 25°C (23). A clean working electrode surface was obtained by abrading the pyrolytic graphite edge surface with P1200 sandpaper and then rinsing with deionised water. Enzyme was adsorbed onto the electrode surface by pipetting on 4 µL of YedY solution and allowing this to dry for approximately 10 min. All values quoted are the average of at least three experiments and the error bars are the standard errors calculated from all repeat data.

Electrochemical Simulations. Simulations of FTacV data were based on a Butler−Volmer formalism for heterogeneous electron transfer kinetics (22) and the mechanism described in the SI Appendix and were performed using the Monash Electrochemistry Simulator (MECSim) digital simulation software package (35). The charge transfer coefficient was assumed to be α = 0.5 in all simulations and all other simulation parameters were optimised to give a close fit between theoretical and experimental data using a heuristic approach.

ACKNOWLEDGMENTS. AP and HA thank the University of York for funding and BBSRC (BB/F017316/1). HA, ANS, AMB and AP also acknowledge Royal Society for funding this work *via* the International Exchange Scheme. We gratefully acknowledge Shannon Murphy's technical assistance in protein purification and thank Prof. Paul Walton and Prof. Anne-Kathrin Duhme-Klair (both University of York) for useful scientific discussions..

1. Hille R, Hall J, & Basu P (2014) The Mononuclear Molybdenum Enzymes. *Chem Rev* 114(7):3963-4038.
2. Hille R (2013) The molybdenum oxotransferases and related enzymes. *Dalton Trans* 42(9):3029-3042.
3. Loschi L, *et al.* (2004) Structural and Biochemical Identification of a Novel Bacterial Oxidoreductase. *J Biol Chem* 279(48):50391-50400.
4. Hitchcock A, *et al.* (2010) Roles of the twin-arginine translocase and associated chaperones in the biogenesis of the electron transport chains of the human pathogen *Campylobacter jejuni*. *Microbiology* 156(10):2994-3010.
5. Rothery R & Weiner J (2015) Shifting the metallocentric molybdoenzyme paradigm: the importance of pyranopterin coordination. *J Biol Inorg Chem* 20(2):349-372.
6. Brokx SJ, Rothery RA, Zhang G, Ng DP, & Weiner JH (2005) Characterization of an *Escherichia coli* Sulfite Oxidase Homologue Reveals the Role of a Conserved Active Site Cysteine in Assembly and Function. *Biochemistry* 44(30):10339-10348.
7. Basu P & Burgmayer SJN (2011) Pterin chemistry and its relationship to the molybdenum cofactor. *Coord Chem Rev* 255(9–10):1016-1038.
8. Havelius KGV, *et al.* (2010) Structure of the Molybdenum Site in YedY, a Sulfite Oxidase Homologue from *Escherichia coli*. *Inorg Chem* 50(3):741-748.
9. Pushie MJ, *et al.* (2010) Molybdenum Site Structure of *Escherichia coli* YedY, a Novel Bacterial Oxidoreductase. *Inorg Chem* 50(3):732-740.
10. Rothery RA, Stein B, Solomonson M, Kirk ML, & Weiner JH (2012) Pyranopterin conformation defines the function of molybdenum and tungsten enzymes. *Proc Natl Acad Sci USA* 109(37):14773-14778.
11. Bond AM, *et al.* (2015) An integrated instrumental and theoretical approach to quantitative electrode kinetic studies based on large amplitude Fourier transformed a.c. voltammetry: A mini review. *Electrochem commun* 57:78-83.
12. Bond AM, Mashkina EA, & Simonov AN (2014) A Critical Review of the Methods Available for Quantitative Evaluation of Electrode Kinetics at Stationary Macrodisk Electrodes. *Developments in Electrochemistry*, (John Wiley & Sons, Ltd), pp 21-47.
13. Guo S, Zhang J, Elton DM, & Bond AM (2003) Fourier Transform Large-Amplitude Alternating Current Cyclic Voltammetry of Surface-Bound Azurin. *Anal Chem* 76(1):166-177.
14. Bond AM, Duffy NW, Guo S-X, Zhang J, & Elton D (2005) Changing the Look of Voltammetry. *Anal Chem* 77(9):186 A-195 A.
15. Simonov AN, *et al.* (2014) New Insights into the Analysis of the Electrode Kinetics of Flavin Adenine Dinucleotide Redox Center of Glucose Oxidase Immobilized on Carbon Electrodes. *Langmuir* 30(11):3264-3273.
16. Fleming BD, Zhang J, Bond AM, Bell SG, & Wong L-L (2005) Separation of Electron-Transfer and Coupled Chemical Reaction Components of Biocatalytic Processes Using Fourier Transform ac Voltammetry. *Anal Chem* 77(11):3502-3510.
17. Léger C & Bertrand P (2008) Direct Electrochemistry of Redox Enzymes as a Tool for Mechanistic Studies. *Chem Rev* 108(7):2379-2438.
18. Yang J, Rothery R, Sempombe J, Weiner JH, & Kirk ML (2009) Spectroscopic Characterization of YedY: The Role of Sulfur Coordination in a Mo(V) Sulfite Oxidase Family Enzyme Form. *J Am Chem Soc* 131(43):15612-15614.
19. Hudson JM, *et al.* (2005) Electron Transfer and Catalytic Control by the Iron−Sulfur Clusters in a Respiratory Enzyme, *E. coli* Fumarate Reductase. *J Am Chem Soc* 127(19):6977-6989.
20. Heering HA, Weiner JH, & Armstrong FA (1997) Direct Detection and Measurement of Electron Relays in a Multicentered Enzyme: Voltammetry of Electrode-Surface Films of *E. coli* Fumarate Reductase, an Iron−Sulfur Flavoprotein. *J Am Chem Soc* 119(48):11628-11638.
21. Hirst J (2006) Elucidating the mechanisms of coupled electron transfer and catalytic reactions by protein film voltammetry. *Biochim Biophys Acta* 1757(4):225-239.
22. Stevenson GP, *et al.* (2012) Theoretical Analysis of the Two-Electron Transfer Reaction and Experimental Studies with Surface-Confined Cytochrome c Peroxidase Using Large-Amplitude Fourier Transformed AC Voltammetry. *Langmuir* 28(25):9864-9877.
23. Bard AJ & Faulkner LR (2010) *Electrochemical Methods: Fundamentals and Applications, 2nd Edition* (Wiley).
24. Armstrong FA, *et al.* (2000) Fast voltammetric studies of the kinetics and energetics of coupled electron-transfer reactions in proteins. *Faraday Discuss* 116(0):191-203.
25. Heffron K, Léger C, Rothery RA, Weiner JH, & Armstrong FA (2001) Determination of an Optimal Potential Window for Catalysis by *E. coli* Dimethyl Sulfoxide Reductase and Hypothesis on the Role of Mo(V) in the Reaction Pathway. *Biochemistry* 40(10):3117-3126.
26. Sabaty M, *et al.* (2013) Detrimental effect of the 6 His C-terminal tag on YedY enzymatic activity and influence of the TAT signal sequence on YedY synthesis. *BMC Biochem* 14(1):1-12.
27. Buc J, *et al.* (1999) Enzymatic and physiological properties of the tungsten-substituted molybdenum TMAO reductase from *Escherichia coli*. *Mol Microbiol* 32(1):159-168.
28. Morris GP, *et al.* (2015) Theoretical Analysis of the Relative Significance of Thermodynamic and Kinetic Dispersion in the dc and ac Voltammetry of Surface-Confined Molecules. *Langmuir* 31(17):4996-5004.
29. Léger C, Jones AK, Albracht SPJ, & Armstrong FA (2002) Effect of a Dispersion of Interfacial Electron Transfer Rates on Steady State Catalytic Electron Transport in [NiFe]-hydrogenase and Other Enzymes. *The Journal of Physical Chemistry B* 106(50):13058-13063.
30. Raghavan R & Dryhurst G (1981) Redox chemistry of reduced pterin species. *J Electroanal Chem Interfacial Electrochem* 129(1–2):189-212.
31. Jacques JGJ, *et al.* (2014) Reductive activation in periplasmic nitrate reductase involves chemical modifications of the Mo-cofactor beyond the first coordination sphere of the metal ion. *Biochim Biophys Acta* 1837(2):277-286.
32. Fleming BD, Barlow NL, Zhang J, Bond AM, & Armstrong FA (2006) Application of Power Spectra Patterns in Fourier Transform Square Wave Voltammetry To Evaluate Electrode Kinetics of Surface-Confined Proteins. *Anal Chem* 78(9):2948-2956.
33. Fleming BD, Zhang J, Elton D, & Bond AM (2007) Detailed Analysis of the Electron-Transfer Properties of Azurin Adsorbed on Graphite Electrodes Using dc and Large-Amplitude Fourier Transformed ac Voltammetry. *Anal Chem* 79(17):6515-6526.
34. Lee C-Y, *et al.* (2011) Theoretical and experimental investigation of surface-confined two-center metalloproteins by large-amplitude Fourier transformed ac voltammetry. *J Electroanal Chem* 656(1–2):293-303.
35. http://www.garethkennedy.net/MECSim.html